


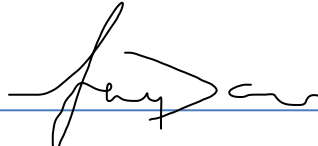
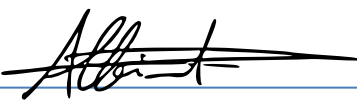




Technical Note on Quality Assessment for FarEarth Landsat 8 OLI RT Products

Author(s): 


Thomas Beaton
Sam Lavender
Christopher Doyle
Task 1 Team

Approval: 
Fay Done
Task 1 Lead

Accepted: 
Clement Albinet
ESA EDAP Technical Officer

AMENDMENT RECORD SHEET

The Amendment Record Sheet below records the history and issue status of this document.

ISSUE	DATE	REASON
0.1	25 November 2020	Draft version for ESA review
0.2	15 June 2021	Draft version for ESA review
1.0	03/08/2021	Final Issue

TABLE OF CONTENTS

1. EXECUTIVE SUMMARY	4
2. INTRODUCTION.....	8
2.1 Reference Documents	8
2.2 Glossary	9
3. EDAP QUALITY ASSESSMENT	11
3.1 EDAP Maturity Matrix.....	11
3.1.1 Product Information	12
3.1.2 Product Generation.....	13
3.1.3 Ancillary Information	13
3.1.4 Uncertainty Characterisation	14
3.1.5 Validation	14
4. EDAP DETAILED QUALITY ASSESSMENT	16
4.1 Objectives.....	16
4.2 Image Quality	16
4.2.1 Activity Description Sheet.....	16
4.2.2 Introduction	16
4.2.3 Image Interpretability	16
4.2.3.1 Methods	17
4.2.3.2 Results	18
4.2.3.2.1 Green Band.....	18
4.2.3.2.2 Red Band	19
4.2.3.2.3 NIR Band.....	20
4.2.3.2.4 SWIR-1 Band	21
4.2.4 Visual Inspection.....	21
4.2.4.1 Methods	21
4.2.4.2 Results	21
4.3 Geometric Calibration Quality	22
4.3.1 Activity Description Sheet.....	22
4.3.2 Introduction	22
4.3.3 Relative Geolocation Accuracy.....	22
4.3.3.1 Method	22
4.3.3.2 Results	23
4.3.4 Absolute Geolocation Accuracy.....	23



4.3.4.1	Method 1	23
4.3.4.2	Results	24
4.3.5	Interband Registration Accuracy	25
4.3.5.1	Method	25
4.3.5.2	Results	25
4.4	Radiometric Calibration Quality.....	27
4.4.1	Activity Description Sheet.....	27
4.4.2	Introduction	28
4.4.3	Methods and Tools	28
4.4.4	Results	29
4.5	Fire Detection Capability Assessment	32
4.5.1	Activity Description Sheet.....	32
4.5.2	Introduction	33
4.5.3	Methods and Tools	34
4.5.4	Fire Classification	34
4.5.5	Results	36
4.5.5.1	Summary statistics.....	36
4.5.5.2	Fire matches	36
4.5.5.2.1	EFFIS matches	36
4.5.5.2.2	Non EFFIS matches.....	36
4.5.5.3	Geolocation Accuracy.....	38
5.	CONCLUSIONS.....	40
APPENDIX A	Test Data: FarEarth and USGS Landsat 8 OLI Products.....	41
A.1	FarEarth Landsat 8 OLI RT products.....	41
A.2	USGS Landsat 8 OLI Products	43

1. EXECUTIVE SUMMARY

Pinkmatter Solutions, an organisation that specialises in the development of real time¹ and near-real² time satellite imagery processing and information extraction algorithms, has developed the FarEarth FireBox algorithm that supports the important provision of a unique, **fire detection in real-time (RT) satellite imagery** service. This service, which is based on the processing chain depicted in Figure 1-1 [RD-1], sees to the application of the aforementioned algorithm to imagery from a satellite pass, during the downlink phase, in order to detect fires as soon as possible (i.e. early warning) and to generate alerts that can then be passed on to the emergency services.

The data quality assessments performed here are, however, primarily focused on comparing the **FarEarth (FE) Fire Landsat 8 (LS8) Operational Land Imager (OLI) RT** products with their nearest native equivalent, the **United States Geological Survey (USGS) L1GS** products, in order to determine the impact on data quality as a consequence of RT processing (i.e. known trade-off between quality and processing time).

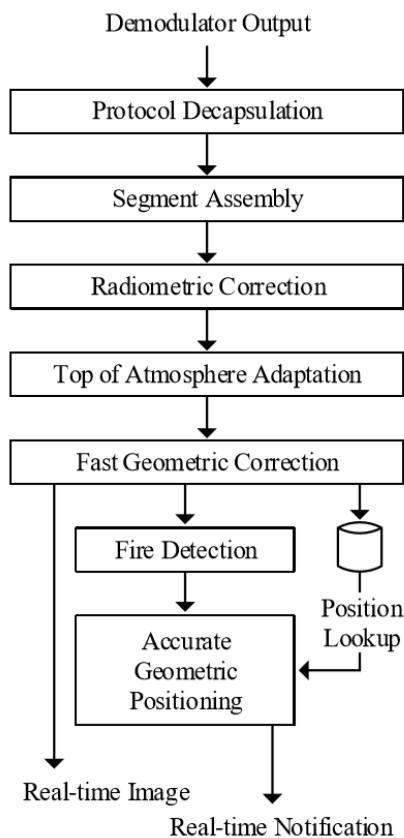


Figure 1-1: Pinkmatter process flow of stream-based processing [RD-1].

Note the geometric and radiometric calibration corrections of a ten minute satellite overpass takes the USGS LS8 OLI processing chain between **thirty and sixty** minutes

¹ RT = defined as a product processed and delivered within 1 hour of acquisition

² NRT = defined as a product processed and delivered within 3 hours of acquisition

and the FE LS8 OLI processing chain **less than ten** minutes (i.e. stream-based approach, which can do the latter corrections whilst the overpass is still in progress).

A summary of the data quality assessments performed on the test dataset of FE LS8 OLI RT products (115 acquisitions, acquired between 29/01/2014 and 12/02/2017) are detailed in Table 1-1. Please note that it is possible that the processing chain used to generate these products has been updated since the assessments described in this document were performed.

Note comparisons are made with [RD-1] as this details the data quality assessments performed by FE using also USGS LS8 L1GS products.

Table 1-1: FE LS8 OLI RT Fire Products: Executive Summary

Assessment Area	Results
Visual Inspection	<p>1. Visual Inspection</p> <p>The visual inspection of the FE LS8 OLI products provided did not reveal any gross anomalies / artefacts.</p>
Image Quality	<p>1. Image Interpretability</p> <p>There appears to be a very slight degradation in image quality, based on factors such as contrast and delineation of objects / features of interest (e.g. delineation of field boundaries and roads), when comparing FE with USGS LS8 OLI products.</p>
Geometric Calibration Quality	<p>Note due to the nature of these products, where a trade-off between data quality and processing time exists, coarse geometric calibration corrections are initially implemented using a systematically calculated sensor model only [RD-1] (i.e. no use of ground control points or a digital elevation model).</p> <p>The ground sampling distance at nadir of LS8 OLI bands is 30.0 m.</p> <p>1. Relative Geolocation Accuracy</p> <p>The relative geolocation accuracy, assessed visually, highlights a large spatial disparity between FE and USGS LS8 OLI products (as expected, confirmed by the assessed absolute geolocation accuracy).</p> <p>2. Absolute Geolocation Accuracy</p> <p>The absolute geolocation accuracy determined using four FE LS8 OLI products is (average) 763.07 m RMSE and (average) 898.10 m CE90.</p>

Assessment Area	Results
	<p>The absolute geolocation accuracy of pixels flagged as fire, which is in the order of that determined above, suggests accurate geometric corrections using attitude, ephemeris and sample time data have not been implemented as expected (accurate geometric processing as depicted in Figure 1-1).</p> <p>3. Interband Registration Accuracy</p> <p>The interband registration accuracy, determined for the green-red and red-near-infrared band band-pairs is comparable to or better than the accuracy determined by [RD-1], and the minimum requirement (0.15 pixels) specified by USGS [RD-7], for the Green-Red and Red-NIR band pairs at 0.022 pixels and 0.015 pixels (RMSE), respectively.</p> <p>However, this does not appear to be the case for the NIR-SWIR-1 band pairs at 1.475 pixels (EDAP) compared to 0.080 pixels (Pinkmatter Solutions) [RD-1]. The reason for this is not known and requires further investigation or the assessment of more FE LS8 OLI products.</p>
<p>Radiometric Calibration Quality</p>	<p>1. Absolute Radiometric Accuracy</p> <p>The absolute radiometric accuracy has been determined through comparisons with reference USGS LS8 OLI L1GS products whose absolute radiometric accuracy is known and well documented (i.e. to support quantification of the radiometric difference). The results of the latter indicate TOA reflectances differences of 2.31% (Green), 5.85% (Red), 12.11% (NIR) and 19.45% (SWIR-1) which are generally higher (i.e. more accurate) than that reported in [RD-1].</p> <p>Without the appropriate metadata or documentation on the FE products, it is not clear if the radiometric information contained in the products is being fully interpreted and so this may account for the differences detailed above. Note the FE LS8 OLI products are radiometrically calibrated and the conversion to scaled top of atmosphere reflectance has already been applied (the conversion of the USGS LS8 OLI products to top of atmosphere reflectance is performed by the user, using the radiometric calibration coefficients provided in the product metadata).</p>
<p>Fire Detection Capability</p>	<p>1. Fire Detection Capability</p> <p>The comparisons made between the FE LS8 OLI products and the Copernicus European Forest Fire Information System (EFFIS) alone revealed a 46.7 % accuracy rating for detecting a fire. This accuracy rating increased to 95.4 % accuracy rating when visual inspections of the FE LS8 OLI product imagery were included (the</p>



Assessment Area	Results
	remaining 4.6 % were found to contain false-positive fire flags due to bright signals present in the imagery).

2. INTRODUCTION

This technical note details the results of the (preliminary) mission data quality assessments (including geometric calibration, radiometric calibration and image quality) performed on a sample of **FE LS8 OLI RT** products procured from CGI.

The aforementioned mission data quality assessments are performed in accordance with the assessment guidelines, detailed in [RD-2, RD-3], that constitute the European Space Agency (**ESA**) Earthnet Data Assessment Pilot (**EDAP**) project's Earth Observation (**EO**) Mission Data Quality Assessment Framework. An important representation of the latter framework, constructed by the National Physical Laboratory (**NPL**), is what is known as the maturity matrix. It is a diagrammatic summary of the following:

- **Documentation Review:** *the EDAP Optical team reviews materials (e.g. data and documentation) provided by the data provider or operator, some of which may not be publically available, or even the scientific community (e.g. published papers). The results are detailed in Section 3 (covering the first four columns of the maturity matrix).*
- **Data Quality Assessments:** *the EDAP Optical team performs the data quality assessments (i.e. validation assessments), independently of any validation assessments performed by the data provider and / or operator. The results are detailed in Section 4 (covering the last column, 'Validation', of the maturity matrix).*

The above assessments are performed by the project's Optical team using the appropriate in-house and open-source ad-hoc scripts / tools.

It is important to note the purpose of the EDAP EO Mission Data Quality Assessment Framework ensures that the delivered commercial mission data is fit for purpose and that all decisions regarding the inclusion of the commercial mission as an ESA third party mission can be made fairly and with confidence.

2.1 Reference Documents

The following is a list of reference documents with a direct bearing on the content of this proposal. Where referenced in the text, these are identified as [RD-n], where 'n' is the number in the list below:

RD-1. Bohme, C., Bouwer, P., Prinsloo, M. Real-Time Stream Processing for Active Fire Monitoring on Landsat 8 Direct reception Data. The International Archives of the Photogrammetry, Remote Sensing and Spatial Information Sciences, Volume XL-7/W3, 2015.

RD-2. EDAP.REP.001 Generic EDAP Best Practice Guidelines,1.1 23 May 2019

RD-3. EDAP.REP.002 Optical Mission Quality Assessment Guidelines, v1.0, 16 October 2019.

RD-4. Wilkinson, M.D., Dumontier, M., Aalbersberg, I.J., Appleton, G., Axton, M., et al. 2016 The FAIR Guiding Principles for scientific data management and stewardship. Scientific Data 3, 160018. (doi:10.1038/sdata.2016.18)

- RD-5. N. A. Bryant., A. L. Zobrist., R. E. Walker and B. Gokhman., An Analysis of Landsat Thematic Mapper P-Product Internal Geometry and Conformity to Earth Surface Geometry., Photogrammetric Engineering and Remote Sensing. Vol.51.No.9.pp.1435-1447.
- RD-6. Gatti, A., Galoppo, A., 14 March 2018. Sentinel-2 Products Specification Document.,<https://sentinels.copernicus.eu/documents/247904/685211/Sentinel-2-Products-Specification-Document.pdf/fb1fc4dc-12ca-4674-8f78-b06efa871ab9?t=1521537947000>
- RD-7. Irons, J.R., Dwyer, J.L. and Barsi, J.A., 2012. The next Landsat satellite: The Landsat data continuity mission. *Remote Sensing of Environment*, 122, pp.11-21.
- RD-8. Meyer, L.H., Heurich, M., Beudert, B., Premier, J., Pflugmacher, D., 2019. Comparison of Landsat-8 and Sentinel-2 Data for Estimation of Leaf Area Index in Temperate Forests. *Remote Sensing*, 11(10), 1160;<https://doi.org/10.3390/rs11101160>
- RD-9. ESA., Copernicus., S2 MPC: L1C Data Quality Report, 55, 07 September 2020.
- RD-10. Helder, D.; Thome, K. J.; Mishra, N.; Chander, G.; Xiong, X.; Angal, A.; Choi, T., 2013. Absolute Radiometric Calibration of Landsat Using a Pseudo Invariant Calibration Site. *IEEE Trans. Remote Sensing*. Vol.51,pp.1360-1369.

2.2 Glossary

The following acronyms and abbreviations have been used in this Report.

EDAP	Earthnet Data Assessment Pilot
EFFIS	Copernicus European Forest Fire Information System
EO	Earth Observation
ESA	European Space Agency
FAIR	Findable, Accessible, Interoperable and Reusable
FE	FarEarth
LS8	Landsat 8
MSI	MultiSpectral Instrument
NPL	National Physical Laboratory
NRT	Near-Real Time
OLI	Operational Land Imager
PICS	Pseudo-Invariant Calibration Sites
RT	Real-Time






S2	Sentinel-2
TOA	Top of Atmosphere
USGS	United States Geological Survey

3. EDAP QUALITY ASSESSMENT

3.1 EDAP Maturity Matrix

Table 3-1: FE LS8 OLI RT Quality Maturity Matrix

Product Information	Product Generation	Ancillary Information	Uncertainty Characterisation	Validation
 Product Details	Sensor Calibration & Characterisation Pre-Flight	Product Flags	Uncertainty Characterisation Method	Reference Data Representativeness
Product Availability & Accessibility	Sensor Calibration & Characterisation Post-Launch	Ancillary Data	Uncertainty Sources Included	Reference Data Quality
 Product Format	Additional Processing		Uncertainty Values Provided	Validation Method
User Documentation			Geolocation Uncertainty	Validation Results
Metrological Traceability Documentation				

Key
Not Assessed
Not Assessable
Basic
Intermediate
Good
Excellent
 Information not public

3.1.1 Product Information

Product Details

Product Details	
Product Name	FarEarth Landsat 8 OLI
Sensor Name	Landsat 8 OLI
Sensor Type	Optical – Multispectral and Panchromatic
Product Version Number	-
Processor Name / Version	Landsat Product Generation System (Pinkmatter)
Product ID	LS8
Processing level of product	Real-Time
Measured Quantity Name	Digital Numbers (DN)
Measured Quantity Units	-
Stated Measurement Quality	None provided
Spatial Resolution	Medium Resolution Green, Red, NIR, SWIR-1: 30.0 m @ Nadir Pan: 15.0 m @ Nadir
Spatial Coverage	Global Coverage (Scene 185 km x 180 km)
Temporal Resolution	16 Days Revisit
Temporal Coverage	2013 – Present (Landsat 8)
Point of Contact	-
Product locator (DOI/URL)	-
Conditions for access and use	Not provided.
Limitations on public access	No public access.
Product Abstract	https://www.pinkmatter.com/farearth-suite

Product Availability and Accessibility

The information provided on product **availability and accessibility** does not meet any of the *Findable, Accessible, Interoperable and Reusable (FAIR) Principles* defined in [RD-4]. Therefore, the status this section of the maturity matrix has been graded as 'Basic'.

Product Format

The **product format** of these products, undocumented by the data provider, do not appear to adopt a standard or well-known product format and they do not contain any form of product metadata. Therefore, the status this section of the maturity matrix has been graded as 'Basic'.

LC81950160442016245MTI00> (Sensor_Path_OrbitNo_Year_DOY_GroundStation)

OLI_Green_native_20160901T101741Z_ 'Tile No'.TIF
OLI_Red_native_20160901T101741Z_ 'Tile No'.TIF
OLI_RED_PAN_20160901T101741Z_ 'Tile No'.TIF
OLI_NIR_native_20160901T101741Z_ 'Tile No'.TIF
OLI_PAN_20160901T101741Z_ 'Tile No'.TIF
OLI_SWIR_native_20160901T101741Z_ 'Tile No'.TIF

FE LS8 OLI RT products are split into ~300 60 x 60 km tiles, each smaller tile split into four individual band (Green, Red, NIR and SWIR-1) and two panchromatic (Pan & Red Pan) GeoTIFF files within a zipped file.

Note the standard USGS and ESA LS8 OLI products contain eleven bands, whereas four bands are included within the FE Fire Detection product (Green, Red, NIR and SWIR-1), as these bands form the basis for FE's Fire Detection indices.

User Documentation

The products procured were not accompanied by (official) **user documentation** but some documentation that users might find useful have been made available online (e.g. [RD-1]). Therefore, this section of the maturity matrix has been graded as *'Basic'*.

Metrological Traceability Documentation

The documentation on **metrological traceability** does not exist, or has not been shared, and therefore, this section of the maturity matrix has been graded as *'Not Assessable'*.

3.1.2 Product Generation

Sensor Calibration and Characterisation Pre-flight

The **sensor calibration and characterisation pre-flight** information is not applicable to this product. Therefore, this section of the maturity matrix has been graded as *'Not Assessable'*.

Sensor Calibration and Characterisation Post-Launch

The **sensor calibration and characterisation post-launch** information is not applicable to this product. Therefore, this section of the maturity matrix has been graded as *'Not Assessable'*.

Additional Processing

The **additional processing** information is documented (very high-level) in [RD-1] only. Therefore, this section of the maturity matrix has been graded as *'Basic'*.

3.1.3 Ancillary Information

Product Flags

This product does not contain **product flags** and, therefore, this section of the maturity matrix has been graded as *'Not Assessable'*.

Ancillary Data

This product does not contain a metadata file, which commonly contains **ancillary data**, and there is no documentation on ancillary data. Therefore, this section of the maturity matrix has been graded as *'Not Assessable'*.

(It is important to note, the latter may be due to the fact that not all ancillary data is available at the time a segment is processed.)

3.1.4 Uncertainty Characterisation

Uncertainty Characterisation Method

There is no information or documentation on **uncertainty characterisation methods** (likely not applicable to this commercial product) and, therefore, this section of the maturity matrix has been graded as *'Not Assessable'*.

Uncertainty Sources Included

There is no information or documentation on **uncertainty sources included** (likely not applicable to this commercial product) and, therefore, this section of the maturity matrix has been graded as *'Not Assessable'*.

Uncertainty Values Provided

There is no information or documentation on **uncertainty values provided** (likely not applicable to this commercial product), other than that found in [RD-1] which refers to those detailed by the USGS, and, therefore, this section of the maturity matrix has been graded as *'Not Assessable'*.

Geolocation Uncertainty

There is no information on **geolocation uncertainty** (i.e. whole mission or per-product) as expected for a real-time product, and, therefore, this section of the maturity matrix has been graded as *'Not Assessable'*.

3.1.5 Validation

Reference Data Representativeness

The reference data representativeness is good but as the sample and variety of reference data used is relatively small, compared with the reference data available, this section of the maturity matrix has been graded as *'Basic'*.

Reference Data Quality

The **reference data quality** from suitable 'gold standard' missions is defined by multiple single uncertainty values for the entire mission and, therefore, this section of the maturity matrix has been graded as *'Intermediate'*.

Validation Method

The **validation methods** used to assess geometric calibration, radiometric calibration and image quality are all well-documented and used by the scientific community (and are confirmed fit for purpose as the results produced are in alignment with what is expected / minimum requirements specified). However, as the validation methods used produce only simple uncertainty values, from a statistical point of view, this section of the maturity matrix has been graded as '*Intermediate*'.

Validation Results

The **validation results** of all data quality assessments are summarised in Section 1.

The validation results generally indicate geometric, radiometric and image qualities that can be considered as better than expected for a real-time product (given the trade-off between quality and processing time). The validation results indicate these qualities are comparable to, or better than, that reported by [RD-1] (e.g. radiometric calibration) but poorer than that demonstrated by their nearest equivalent products (USGS LS8 OLI L1GS products) (e.g. geometric calibration). However, it is important to note that the latter results could not be reliably justified or explained in detail as FE product metadata or documentation (except for [RD-1]) does not exist or is not made available. Therefore, this section of the maturity matrix has been graded as "*Intermediate*".

4. EDAP DETAILED QUALITY ASSESSMENT

4.1 Objectives

The primary objective of this work is to assess all core data quality aspects (geometric calibration, radiometric calibration and image quality) of the FE LS8 OLI RT products provided by the data provider. The secondary objective of this work is to assess the latter data quality against the data quality of their nearest native equivalent, USGS LS8 OLI L1GS products (systematic geometric, using spacecraft ephemeris data, and radiometric corrections only).

Note the implemented processing is intended to enable the detection fires in real-time but the drawback of providing this imagery is reduced data quality, expected as a result of the need to minimise processing time. Therefore, the data quality assessments of these products should take the latter into consideration.

4.2 Image Quality

4.2.1 Activity Description Sheet

Image Quality
<i>Inputs</i>
115 Level 1 FE LS8 OLI RT tiles over La Crau and Libya. Reference USGS LS8 L1GS product: LC08_L1GS_197030_20160729_20170322_01_T1
<i>Description</i>
<ul style="list-style-type: none"> Assess the image interpretability of the full-resolution imagery in both FE and USGS products (for comparison). Assess (visual inspection) the full-resolution imagery in the FE products for any gross-anomalies or artefacts.
<i>Outputs</i>
The qualitative assessment of image quality.

4.2.2 Introduction

The image quality assessments performed here include **image interpretability** (section 4.2.3) and **visual inspection** (section 4.2.4).

4.2.3 Image Interpretability

The image interpretability of optical sensor imagery is an important aspect of image quality (originating from the actual sensor or image processing), especially in terms of their practical use or application. This is commonly assessed, subjectively, using well-defined procedures that are based on the successful interpretation of objects or features.

4.2.3.1 Methods

The method adopted here consists of clipping full-resolution imagery, from both products, centred on points of interest (natural and artificial objects or features) that have been deemed suitable for the spatial resolution of these products. The clips, for each band, are then compared to see if degradation in image interpretability exists.

The points of interest used for this assessment are found in the south of France (locations are shown in Figure 4-1 and detailed in Table 4-1).

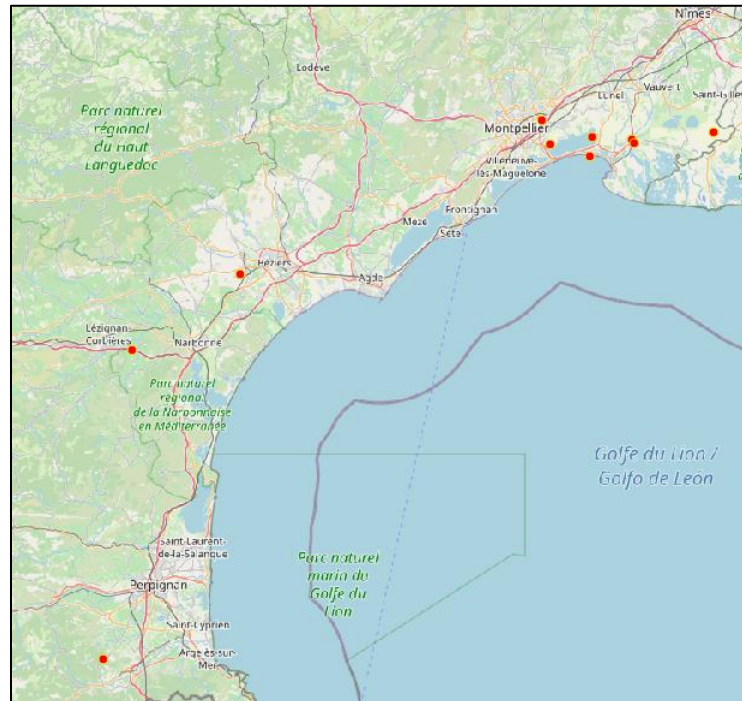


Figure 4-1: Image Interpretability POI Distribution for South of France.

Table 4-1: POI list for Narbonne.

Wkgt_geom UTM31	ID	Description
596553.207589393365197, 4826864.913647760637105	1	Bridge / River*
596857.959435537457466, 4825846.400898804888129	2	Road Intersection*
614453.36865765217226, 4828709.464295474812388	3	Field Array 1
587284.67334163445048, 4822926.745101749897003	4	Port
587713.180046731024049, 4827086.012019109912217	5	Flood Defences
578262.44500955415424, 4825560.685399131849408	6	Airport
576548.418189167510718, 4830812.840977197512984	7	Woodland
485744.309250435617287, 4779415.623890653252602	8	Highway
479053.314644248050172, 4710657.988366433419287	9	Suburban / Forest
509905.797411205072422, 4796375.054402460344136	10	Field Array 2

*ID 1 & 2 are located within the same AOI

4.2.3.2 Results

4.2.3.2.1 Green Band

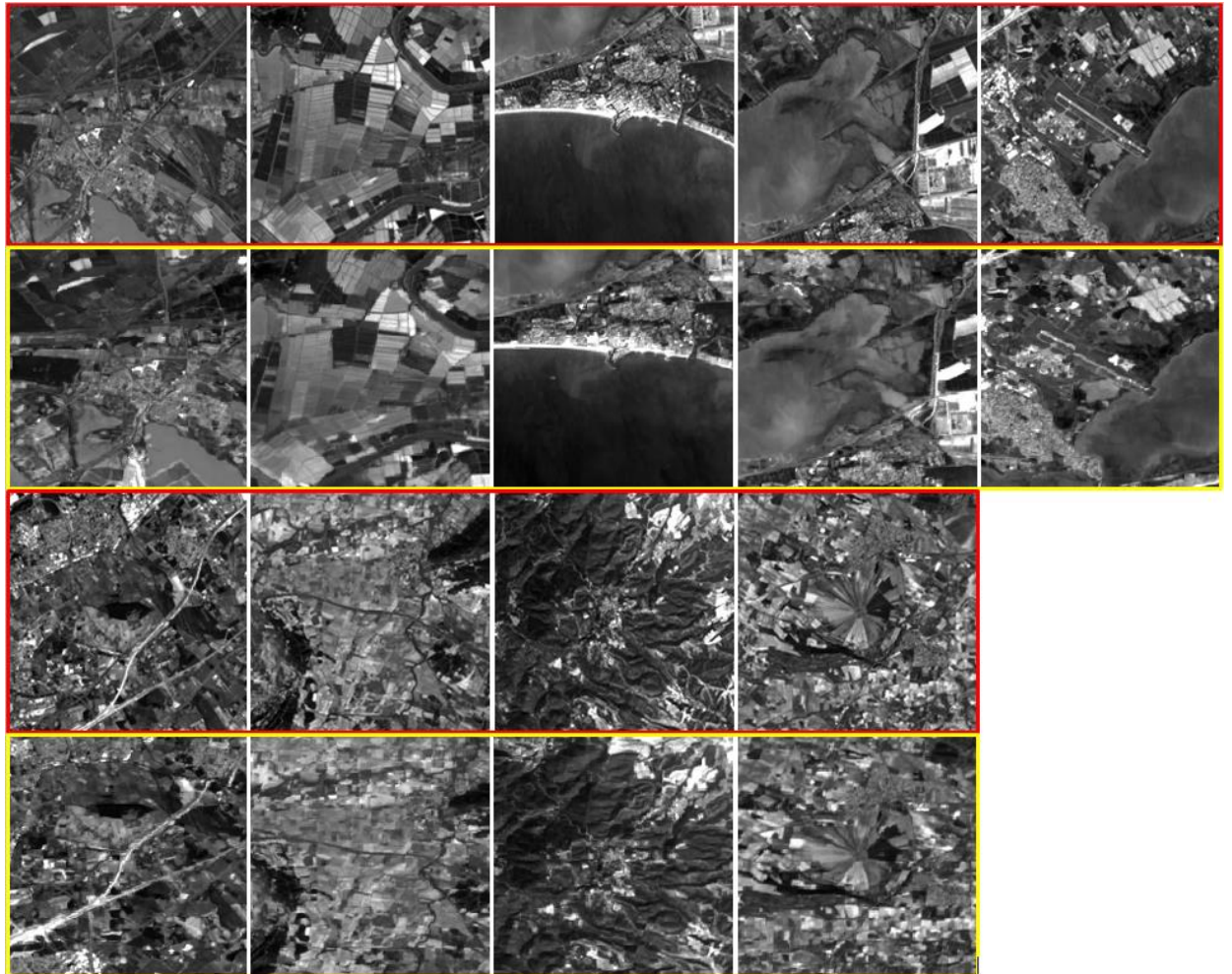


Figure 4-2: Image interpretability difference between USGS (Red Boundary) and FE (Yellow Boundary) products.

4.2.3.2.2 Red Band

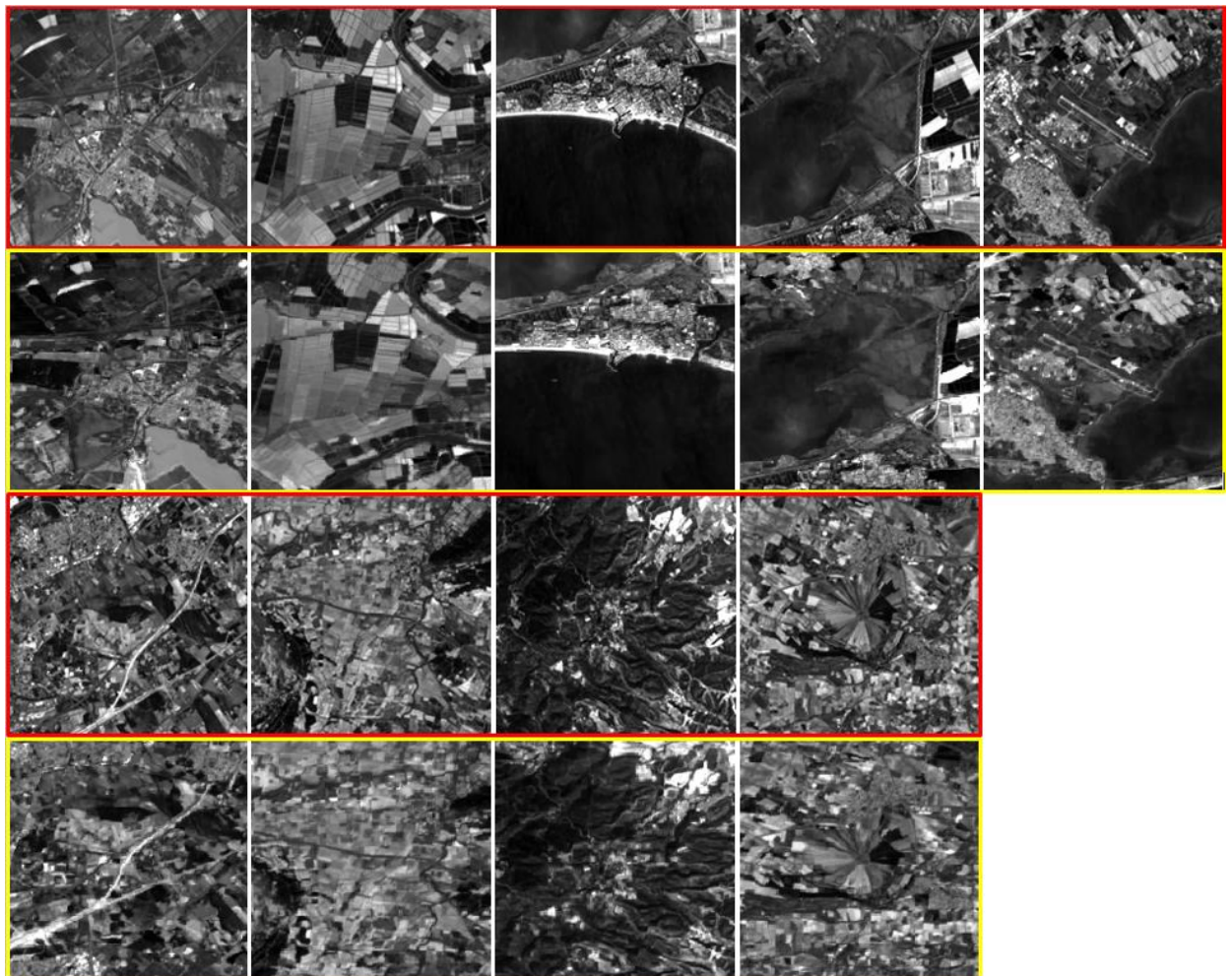


Figure 4-3: Image interpretability difference between USGS (Red Boundary) and FE (Yellow Boundary) products.

4.2.3.2.3 NIR Band

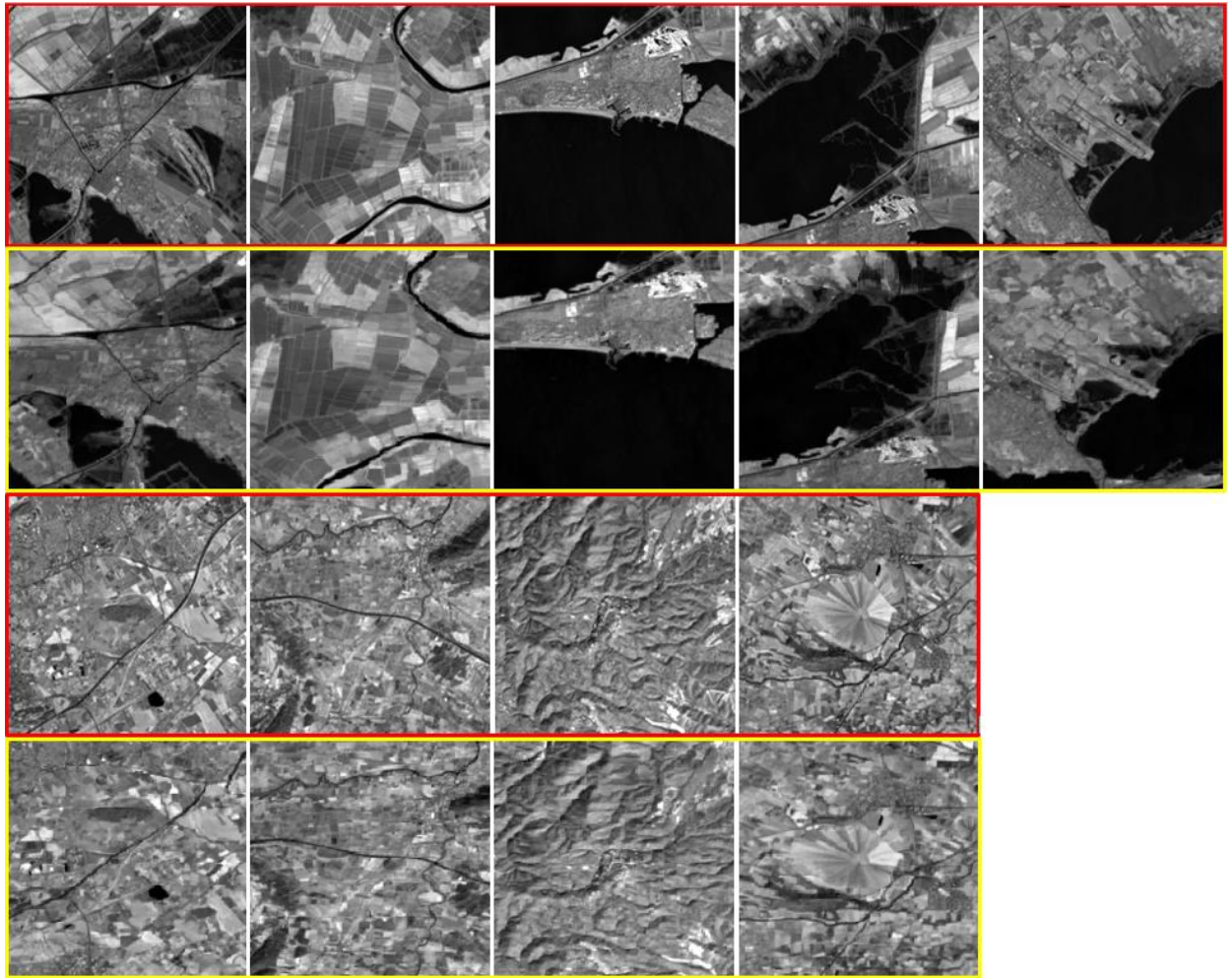


Figure 4-4: Image interpretability difference between USGS (Red Boundary) and FE (Yellow Boundary) products.

4.2.3.2.4 SWIR-1 Band

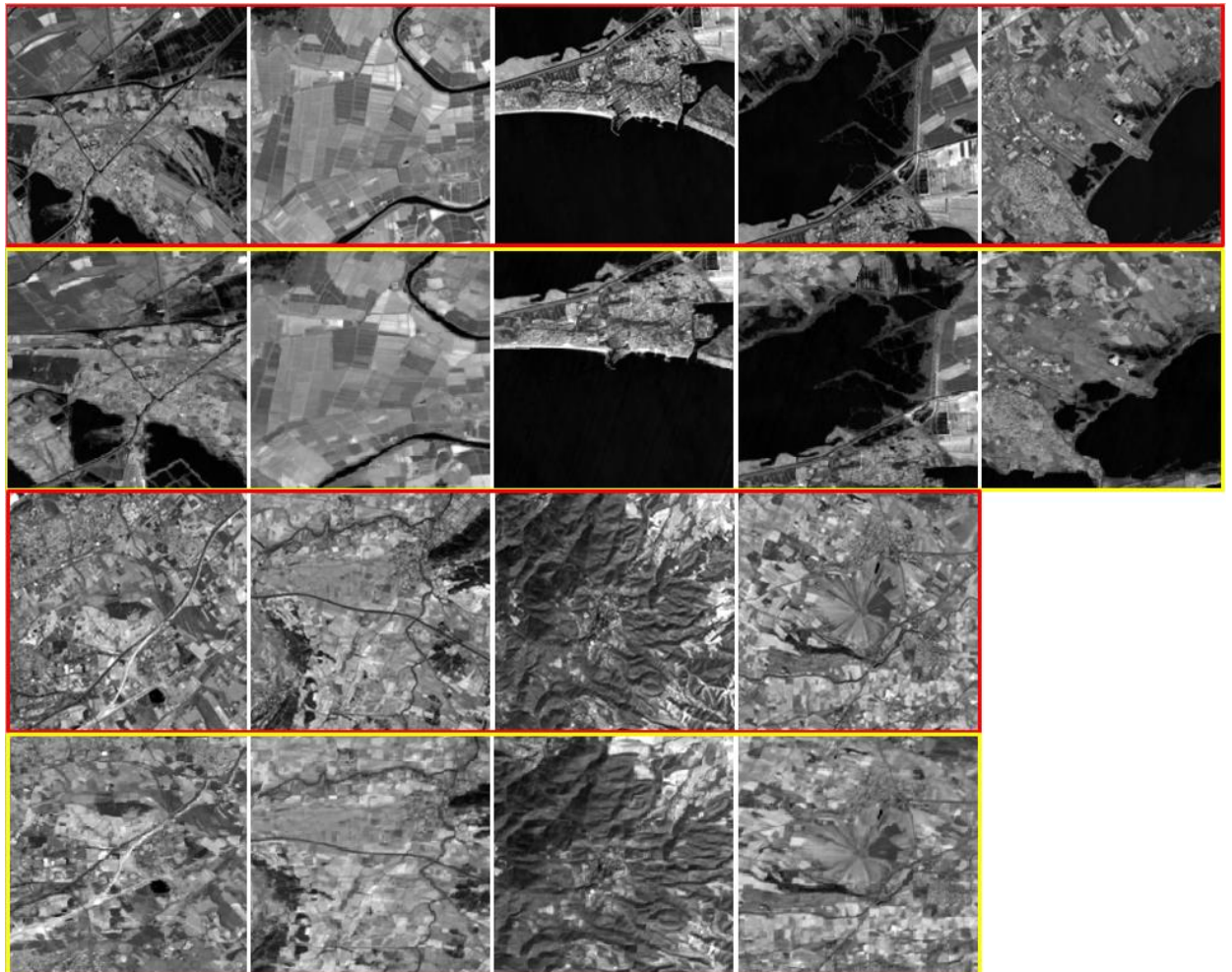


Figure 4-5: Image interpretability difference between USGS (Red Boundary) and FE (Yellow Boundary) products.

The results above generally indicate a slight degradation in image quality, in terms of image interpretability, as better levels of texture, contrast and sharpness, which allow for the interpretation (delineation) of points of interest, are found in the USGS products than in the FE products. Note there were some points of interest, including field boundaries and roads that could be delineated in the USGS products but not the FE products.

4.2.4 Visual Inspection

4.2.4.1 Methods

The product imagery was visually inspected for gross anomalies or artefacts using QGIS.

4.2.4.2 Results

The results of the visual inspection did not reveal any gross anomalies or artefacts.

4.3 Geometric Calibration Quality

4.3.1 Activity Description Sheet

Geometric Calibration Quality: Relative / Absolute / Interband Registration
<i>Inputs</i>
<ol style="list-style-type: none"> 1. FE LS8 OLI RT tiles. 2. USGS LS8 OLI L1GS reference tile (LC08_L1GS_197030_20160729_20170322_01_T1). 3. Sentinel-2 L1C MSI reference tile (S2A_MSIL1C_20200904T104031_N0214_R008_T31TEJ_20200904T133113)
<i>Description</i>
<p>Estimate the relative geolocation accuracy and absolute geolocation accuracy, using imagery from a reference product, and interband registration accuracy. Verify the determined accuracies against metrics described in [RD-1, RD-5, RD-8].</p> <p>Note the following performance metrics should be taken into consideration:</p> <ul style="list-style-type: none"> • Absolute Geolocation Accuracy <ul style="list-style-type: none"> ○ USGS LS8 L1C Products < 12.0 m (RMSE) [RD-7]; ○ USGS LS8 L1GS Products < unknown (RMSE); ○ S2A MSI L1C Products (without ground control points) < 11.0 m (RMSE) [RD-9]. • Interband Accuracy <ul style="list-style-type: none"> ○ FE LS8 RT Products < 0.1 Pixels (mean error, easting and northing directions). <p>Pixel size given is 30.0 m.</p>
<i>Outputs</i>
Geometric calibration accuracies.

4.3.2 Introduction

The geometric calibration quality assessments performed here include **relative geolocation accuracy**, **absolute geolocation accuracy** and **interband registration accuracy**.

4.3.3 Relative Geolocation Accuracy

4.3.3.1 Method

The relative geolocation accuracy assessment, which provides a simple (early) assessment of geolocation accuracy, is based on the comparison of imagery from the FE

products to reference imagery from the USGS products. The method used involves the creation of compressed checkerboard imagery (with transparent squares), from the original imagery of each band of the FE product, which is then laid on top of reference band imagery. The use of the QGIS transparency function then enables the viewing and matching of permanent structures, e.g. roads and bridges, for the input products used.

4.3.3.2 Results

The results indicate a clear geometric disparity, as shown in Figure 4-6, in the order of approximately 800.0 m. The latter result, determined using a measuring tool provided by QGIS, is not comparable to the geolocation accuracy of the USGS L1GS products (where, for both, geometric refinement, including corrections for terrain, have not been implemented).

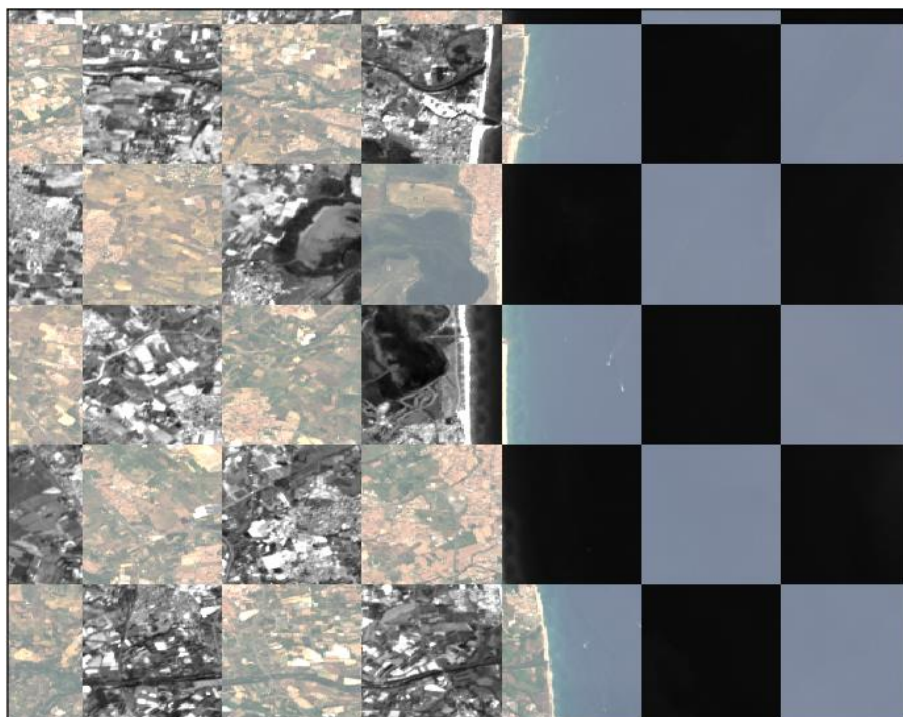


Figure 4-6: Checkerboard FE LS8 OLI RT Green band overlaid on a RGB USGS LS8 OLI L1GS reference image (Narbonne, France).

4.3.4 Absolute Geolocation Accuracy

4.3.4.1 Method 1

The absolute geolocation accuracy is determined using ground control points derived from the S2 MSI L1C reference imagery, whose absolute geolocation accuracy is known, over Narbonne (France) and Butnan (Libya). Note only those ground control points within an elevation range of 0.0 – 30.0 m (above sea level), as indicated by using a digital elevation model, were used in order to limit geometric processing variability by limiting topographic variability.

(RD-6 gives detailed geometric information for S2 reference products used to produce the ground control points dataset to compute the across-track (easting direction) / along-track (northing direction) geometric statistics.)

4.3.4.2 Results

The results of the absolute geolocation assessment are detailed in Table 4-2; the (average) absolute geolocation accuracy for the FE products is 763.07 m RMSE and 898.10 m CE90. Note the absolute geolocation accuracy minimum requirement has not been specified by the data provider.

Table 4-2: Absolute geolocation accuracy of FE LS8 OLI RT products using S2 MSI L1C products as reference.

Parameter	Value	
	Butnan	Narbonne
Mean Easting Error (m)	697.49	679.37
Mean Northing Error (m)	-244.14	-187.30
Easting Error Standard Deviation (m)	738.98	704.71
Northing Error Standard Deviation (m)	260.97	233.63
Root Mean Squared Error (m)	783.71	742.43
Circular Error (CE90 m)	902.96	893.25

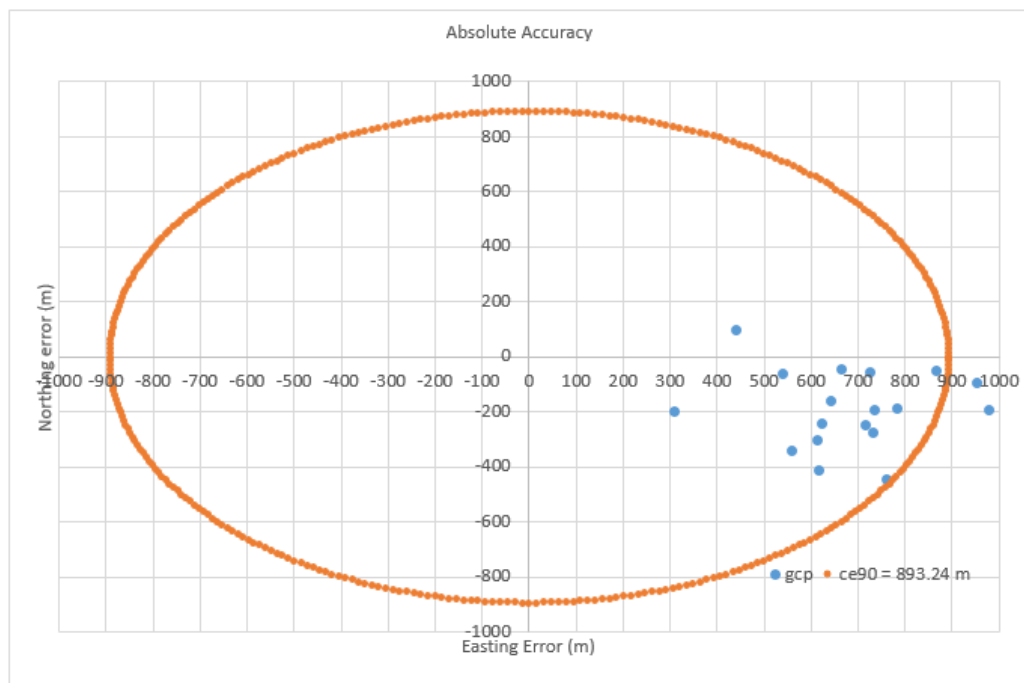


Figure 4-7: Absolute Geolocation Accuracy (Narbonne).

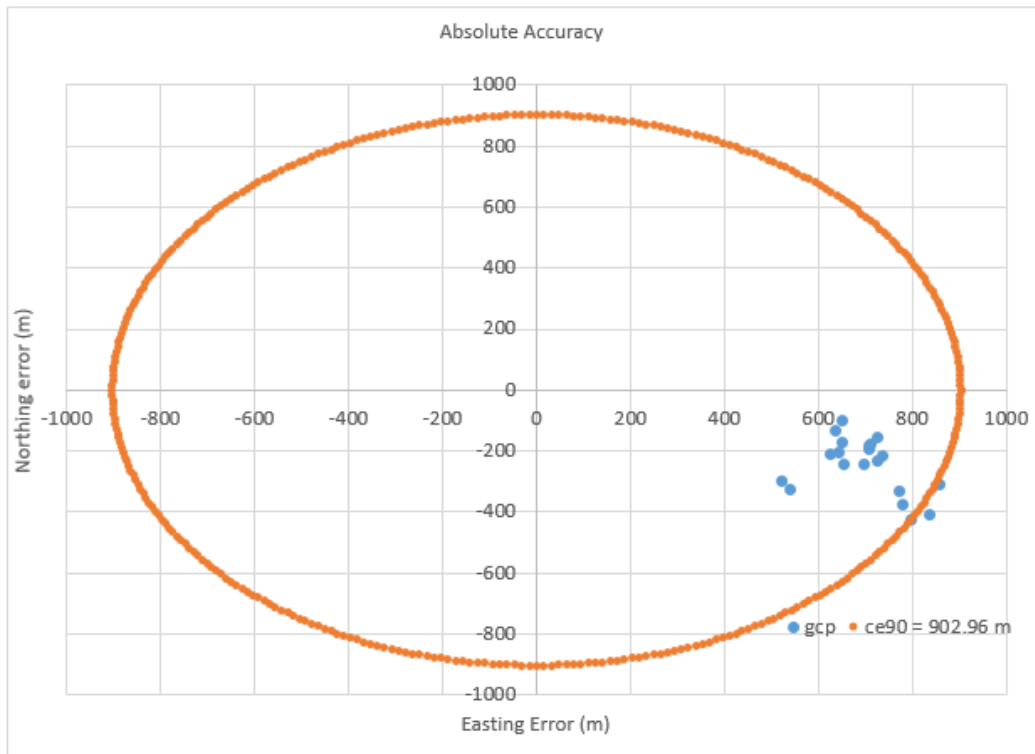


Figure 4-8: Absolute Geolocation Accuracy (Libya).

4.3.5 Interband Registration Accuracy

4.3.5.1 Method

The interband registration accuracy assessment is performed, using an open source intensity-based image matching algorithm / tool provided³, on all adjacent multispectral band pairs present in the imagery of the FE products only.

Note the panchromatic band has not been included in this assessment as its adjacent band pairs are not included in the imagery (and the spatial resolutions differ significantly (i.e. shortwave-infrared 2 is 30 m, panchromatic is 15 m and cirrus is 100 m) and so the error introduced by geometric resampling would be significant).

4.3.5.2 Results

The results of the interband registration accuracy assessment are detailed in Table 4-3. The results indicate the following:

- The mean error in the easting and northing directions, for all adjacent bands, is less than 0.05 pixels (1.5 m) and -1.05 pixels (31.5 m), respectively. The precision in the easting and northing directions, described by the standard deviation, is 0.27 pixels (8.10 m) and 1.36 pixels (40.8 m), respectively.

³ CNES Medicis / QPEC tool

- The interband registration accuracy (root mean square error) is 0.022 (0.66 m), 0.015 (0.45 m) and 1.475 (44.25 m) pixels for the green-red, red-NIR and NIR-SWIR-1 band pairs, respectively. The registration accuracy of the last band pair is poor and the reason for this is unknown but more products should be assessed in order to confirm this.
- The mean error and standard deviations of the interband registration accuracies are detailed in Table 4-3 and they indicate that they are slightly higher (better) than those determined in [RD-1]. This might be due to the different tool(s) or acquisition(s) used to determine this.

Note image-matching was performed at 2 sigma (95%) confidence level.

Table 4-3: Results of the interband registration accuracy assessment, including comparisons with those detailed in [RD-1].

	EDAP			RD-1		
	GREEN v RED	RED v NIR	NIR v SWIR-1	GREEN v RED	RED v NIR	NIR v SWIR-1
MEAN EASTING ERROR (px)	0.007	-0.003	0.050	0.033	0.016	0.027
MEAN EASTING ERROR STD (px)	0.106	0.137	0.274	0.065	0.139	0.153
EASTING RMSE (px)	0.006	0.009	0.039	0.003	0.010	0.012
MEAN NORTHING ERROR (px)	-0.046	0.048	-1.046	0.093	0.062	0.040
MEAN NORTHING ERROR STD (px)	0.200	0.144	1.362	0.233	0.390	0.396
NORTHING RMSE (px)	0.021	0.011	1.474	0.031	0.078	0.079
RMSE (px)	0.022	0.015	1.475	0.032	0.079	0.080
CE90 (m)	9.710	7.830	46.026	-	-	-

- The interband registration accuracy is lower in the northing direction than in the easting direction and this may be due to the distortions indicated in Figure 4-9 (i.e. two peaks in the distribution of displacement). The latter may be a factor of the FE RT processing, conducted on variable size image segments assembled from detector lines of the push broom sensor [RD-1] as they are streamed from the satellite.

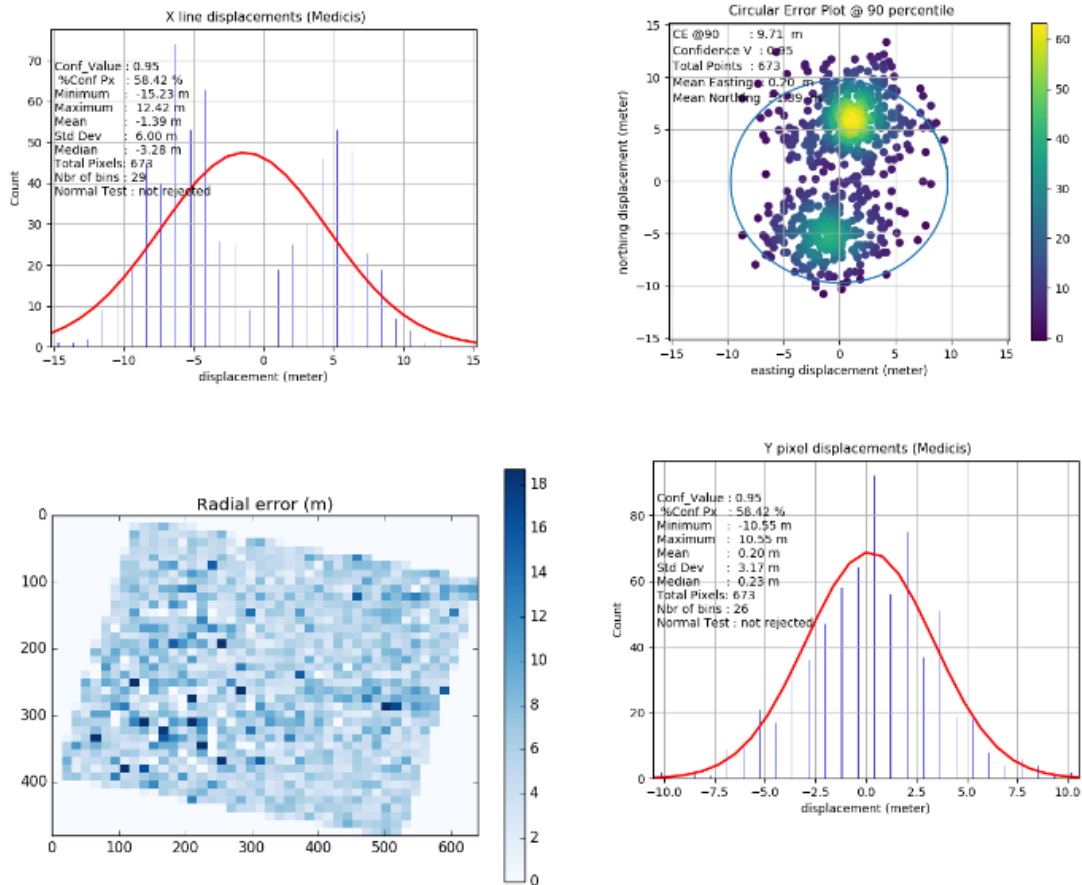


Figure 4-9: The results of the Green-Red band registration accuracy using the image matching tool.

4.4 Radiometric Calibration Quality

4.4.1 Activity Description Sheet

Radiometric Calibration Quality	
<i>Inputs</i>	40 FE LS8 OLI RT and USGS LS8 OLI L1GS products (Table 4-4) 0.5° latitude / longitude polygon ROI
<i>Description</i>	Assess the radiometric agreement between FE and USGS products over Pseudo-Invariant Calibration site (PICS) using the aforementioned polygon ROI. Note the radiometric calibration accuracy should be independent of the processing level.
<i>Outputs</i>	The radiometric agreement, or offset, between FE and USGS products.

4.4.2 Introduction

Without documentation or metadata, the radiometric calibration quality of FE products is determined through quantifying their agreement with the reference USGS products (calibration and validation of USGS LS8 OLI products are well known / documented). Note same-day acquisitions over Libya-4 are used in order to ensure that there are no variables outside of image processing that could influence the differences observed in Top of Atmosphere (TOA) reflectance measurements.

4.4.3 Methods and Tools

The method used for this assessment consists of the following steps (per product listed in Table 4-4):

1. Perform the DN to TOA reflectance conversion for the USGS products, using the radiometric calibration / rescaling coefficients provided in the product metadata. (Note the DN to TOA reflectance conversion has already been performed for FE products.)
2. Derive the mean TOA reflectance from the TOA reflectances extracted from the 0.5° latitude / longitude polygon ROI over PICS Libya-4 (as shown in Figure 4-10).

The radiometric difference between these products can be estimated by comparing the mean TOA derived for all FE products assessed with the mean TOA derived for all USGS products assessed (see Table 4-4).

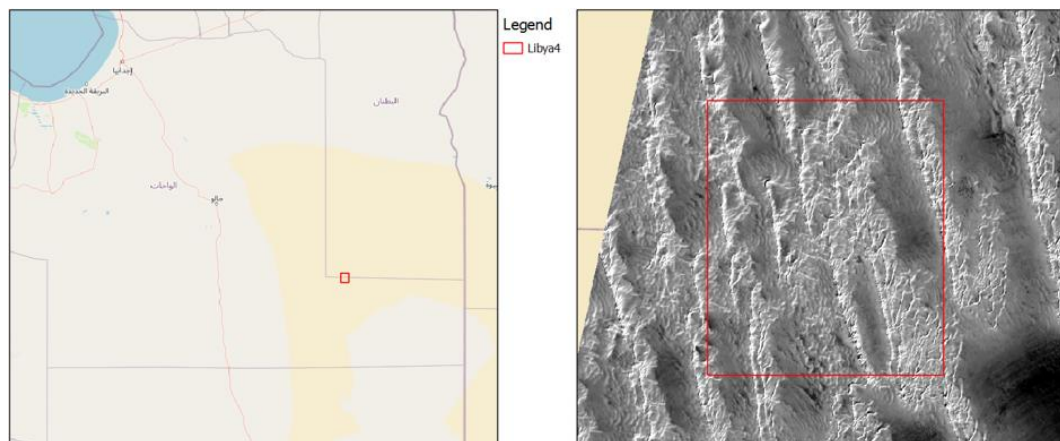


Figure 4-10: Half-degree Libya 4 PICS site used for the radiometric agreement assessment.

Table 4-4: A list of LS8 FE and USGS reference products used for the radiometric assessment.

Date	FE Product ID	USGS Product ID
29/01/2014	LS8_OLI_20140129T085630Z	LC08_L1GS_181040_20140129_20170426_01_T1
02/03/2014	LS8_OLI_20140302T085601Z	LC08_L1GS_181040_20140302_20170425_01_T1
03/04/2014	LS8_OLI_20140403T085537Z	LC08_L1GS_181040_20140403_20170424_01_T1
22/06/2014	LS8_OLI_20140622T085508Z	LC08_L1GS_181040_20140622_20170421_01_T1
08/07/2014	LS8_OLI_20140708T085515Z	LC08_L1GS_181040_20140708_20170421_01_T1
24/07/2014	LS8_OLI_20140724T085517Z	LC08_L1GS_181040_20140724_20170421_01_T1
09/08/2014	LS8_OLI_20140809T085527Z	LC08_L1GS_181040_20140809_20170420_01_T1
25/08/2014	LS8_OLI_20140825T085529Z	LC08_L1GS_181040_20140825_20170420_01_T1
10/09/2014	LS8_OLI_20140910T085533Z	LC08_L1GS_181040_20140910_20170419_01_T1

26/09/2014	LS8_OLI_20140926T085531Z	LC08_L1GS_181040_20140926_20170419_01_T1
28/10/2014	LS8_OLI_20141028T085535Z	LC08_L1GS_181040_20141028_20170418_01_T1
29/11/2014	LS8_OLI_20141129T085537Z	LC08_L1GS_181040_20141129_20170417_01_T1
31/12/2014	LS8_OLI_20141231T085526Z	LC08_L1GS_181040_20141231_20170415_01_T1
17/02/2015	LS8_OLI_20150217T085513Z	LC08_L1GS_181040_20150217_20170412_01_T1
05/03/2015	LS8_OLI_20150305T085508Z	LC08_L1GS_181040_20150305_20170412_01_T1
21/03/2015	LS8_OLI_20150321T085458Z	LC08_L1GS_181040_20150321_20170411_01_T1
06/04/2015	LS8_OLI_20150406T085447Z	LC08_L1GS_181040_20150406_20170410_01_T1
22/04/2015	LS8_OLI_20150422T085446Z	LC08_L1GS_181040_20150422_20170409_01_T1
08/05/2015	LS8_OLI_20150508T085430Z	LC08_L1GS_181040_20150508_20170409_01_T1
24/05/2015	LS8_OLI_20150524T085428Z	LC08_L1GS_181040_20150524_20170408_01_T1
09/06/2015	LS8_OLI_20150609T085439Z	LC08_L1GS_181040_20150609_20180527_01_T1
25/06/2015	LS8_OLI_20150625T085444Z	LC08_L1GS_181040_20150625_20170407_01_T1
11/07/2015	LS8_OLI_20150711T085457Z	LC08_L1GS_181040_20150711_20170407_01_T1
27/07/2015	LS8_OLI_20150727T085502Z	LC08_L1GS_181040_20150727_20170406_01_T1
28/08/2015	LS8_OLI_20150828T085514Z	LC08_L1GS_181040_20150828_20170405_01_T1
13/09/2015	LS8_OLI_20150913T085521Z	LC08_L1GS_181040_20150913_20170404_01_T1
15/10/2015	LS8_OLI_20151015T085526Z	LC08_L1GS_181040_20151015_20170403_01_T1
31/10/2015	LS8_OLI_20151031T085532Z	LC08_L1GS_181040_20151031_20170402_01_T1
02/12/2015	LS8_OLI_20151202T085534Z	LC08_L1GS_181040_20151202_20170401_01_T1
24/04/2016	LS8_OLI_20160424T085456Z	LC08_L1GS_181040_20160424_20170326_01_T1
11/06/2016	LS8_OLI_20160611T085507Z	LC08_L1GS_181040_20160611_20170324_01_T1
13/07/2016	LS8_OLI_20160713T085522Z	LC08_L1GS_181040_20160713_20170323_01_T1
29/07/2016	LS8_OLI_20160729T085526Z	LC08_L1GS_181040_20160729_20180527_01_T1
30/08/2016	LS8_OLI_20160830T085536Z	LC08_L1GS_181040_20160830_20170321_01_T1
01/10/2016	LS8_OLI_20161001T085540Z	LC08_L1GS_181040_20161001_20170320_01_T1
17/10/2016	LS8_OLI_20161017T085546Z	LC08_L1GS_181040_20161017_20170319_01_T1
02/11/2016	LS8_OLI_20161102T085547Z	LC08_L1GS_181040_20161102_20170318_01_T1
04/12/2016	LS8_OLI_20161204T085545Z	LC08_L1GS_181040_20161204_20170317_01_T1
20/12/2016	LS8_OLI_20161220T085540Z	LC08_L1GS_181040_20161220_20180527_01_T1
05/01/2017	LS8_OLI_20170105T085539Z	LC08_L1GS_181040_20170105_20170312_01_T1

4.4.4 Results

According to [RD-1], FE does apply several radiometric corrections to the real-time data in terms of bias removal, response linearisation, gain application and relative top of atmosphere. These corrections are simplified and finer corrections are ignored for the application of real-time processing, finding a reasonable balance between accuracy and processing-time. Considering the above, the radiometric accuracy is defined by the observed radiometric difference of 2.31% (Green), 5.85% (Red), 12.11% (NIR) and 19.45%

(SWIR-1) TOA reflectance values between FE and USGS products (see Table 4-5,

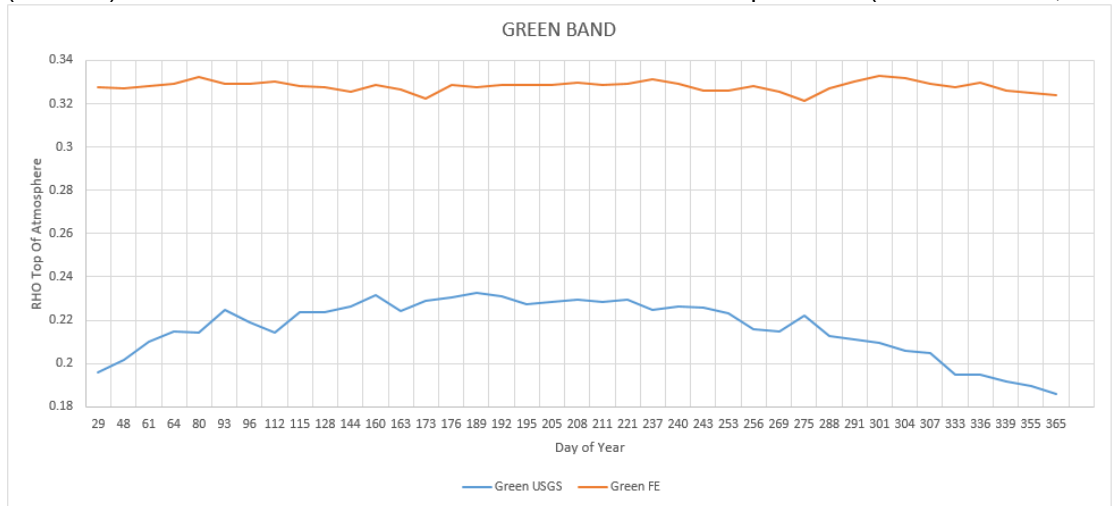


Figure 4-11 to

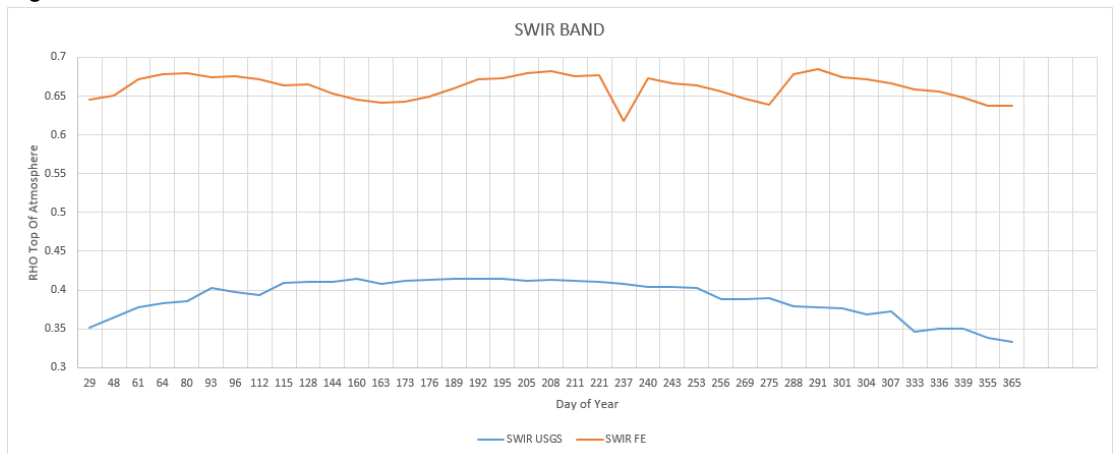


Figure 4-14). The latter differences in the NIR and SWIR-1 bands indicate a degradation in radiometric calibration quality but the reason for this is not clear – it may be due to the different radiometric calibration algorithms used (FE used an adaptation of the USGS OLI radiometric algorithm [RD-1]).

Table 4-5: Mean and standard deviation values across Green, Red, NIR and SWIR bands for FE real-time and USGS L1GS products.

	GREEN BAND		RED BAND		NIR BAND		SWIR-1 BAND	
	MEAN	STD	MEAN	STD	MEAN	STD	MEAN	STD
FE	0.328	0.002	0.447	0.004	0.569	0.007	0.662	0.016
USGS	0.265	0.042	0.362	0.058	0.461	0.075	0.542	0.092
FE Offset (%)	2.31		5.85		12.11		19.45	

However, the observed radiometric differences are higher (i.e. more accurate) than that reported in [RD-1] – 5.67 % (Green), 8.66 % (Red), 17.64 % (NIR) and 29.76 % (SWIR-1).

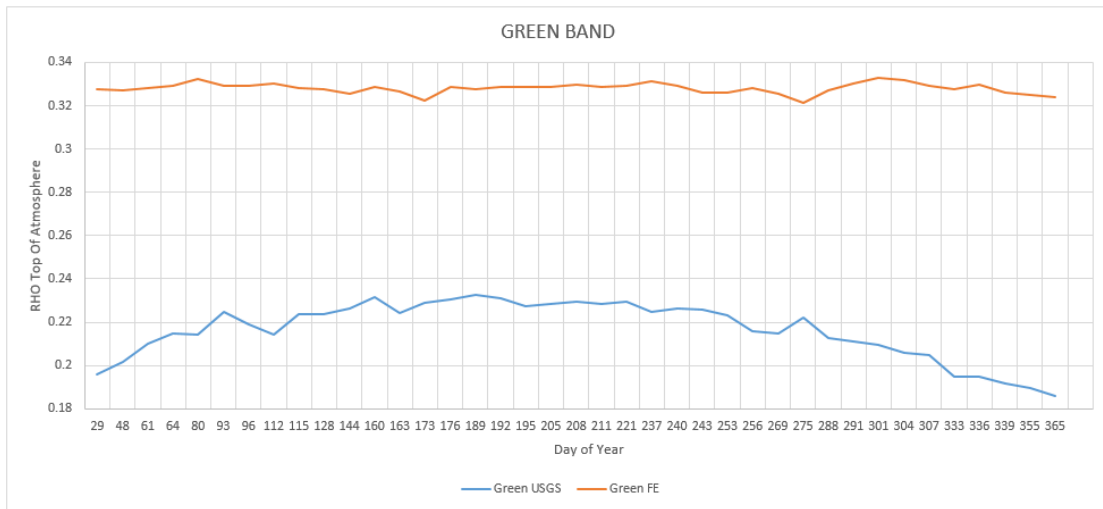


Figure 4-11: The radiometric difference between the FE and USGS products, for the Green band, can be observed from this time-series of TOA reflectance.

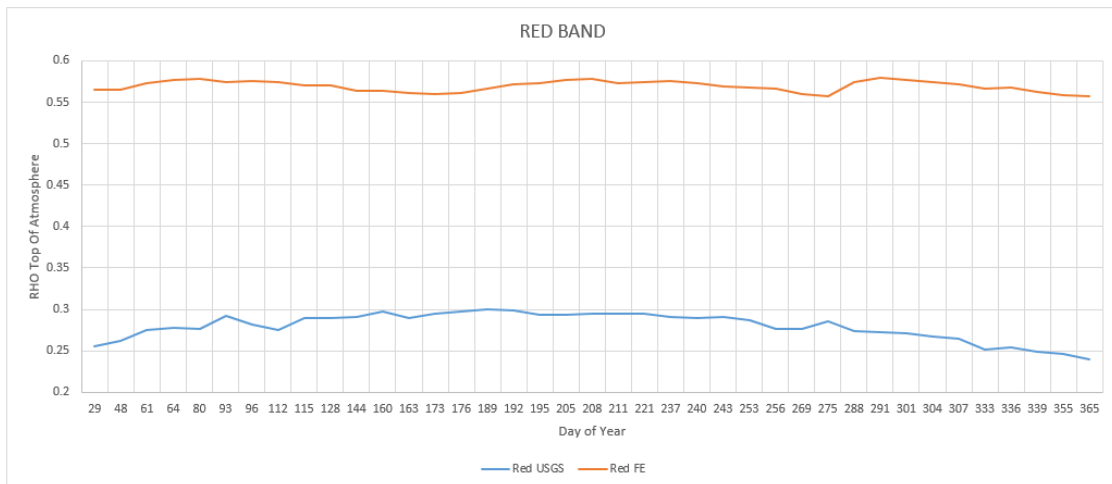


Figure 4-12: The radiometric difference between the FE and USGS products, for the Red band, can be observed from this time-series of TOA reflectance.

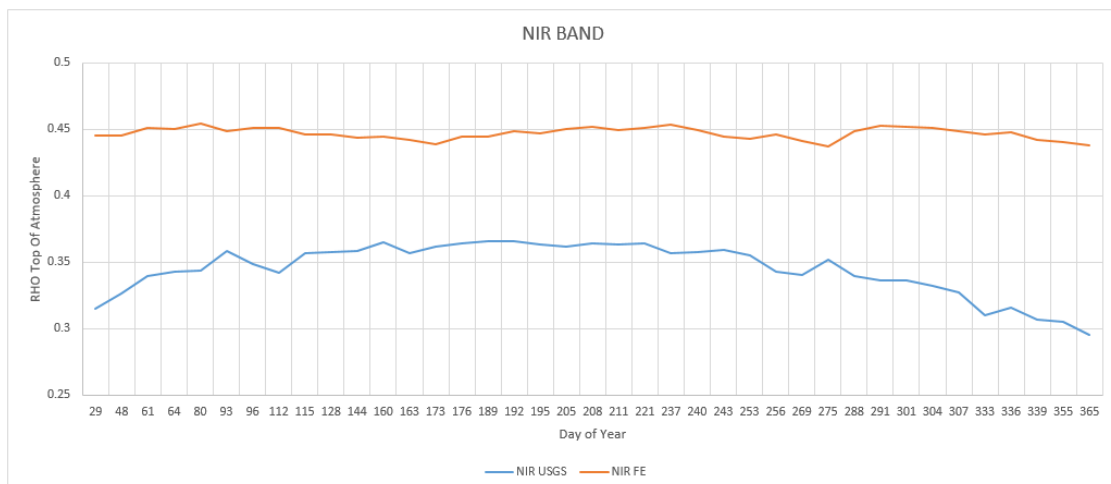


Figure 4-13: The radiometric difference between the FE and USGS products, for the NIR band, can be observed from this time-series of TOA reflectance.

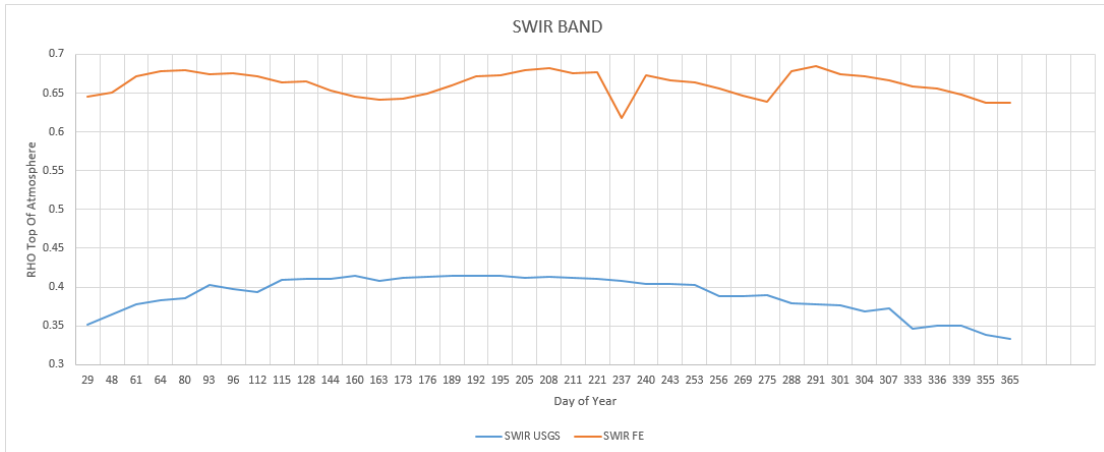


Figure 4-14: The radiometric difference between the FE and USGS products, for the red band, can be observed from this time-series of TOA reflectance.

There appears to be a near consistent difference, for each band, which may suggest a bias or constant factor is missing from radiometric calibration of the data.

The time-series also show differences in temporal radiometric variability, calculated by dividing the standard deviation by the mean TOA reflectance, throughout the year. The temporal radiometric variability, detailed in Table 4-6, is relatively small for each band but some annual variations that you would expect, even very small variations in observations over PICS, is seen in the time-series of USGS products but not FE products.

Table 4-6: Temporal radiometric variability of FE and USGS LS8 OLI products, expressed as %.

	Green	Red	NIR	SWIR-1
FE	0.74	1.16	0.99	2.39
USGS	0.40	0.41	0.42	0.44
FE Offset	0.34	0.75	0.57	1.95

4.5 Fire Detection Capability Assessment

It is important to note that LS8 alone is not suitable for operational fire monitoring due to its 16-day revisit cycle, but it has been chosen by the Pinkmatter Solutions to illustrate only this real-time, stream-based processing approach with a fire detection use case.

4.5.1 Activity Description Sheet

FE Fire Product accuracy analysis
Inputs

1 set of FE KML scenes, EFFIS database of active fire markers, LS7 and LS8 SWIR bands
<i>Description</i>
The scope of this activity was to compare FE LS8 OLI RT fire products against the Copernicus EFFIS fire markers and conduct visual product inspections to assess the accuracy of the fire product.
<i>Outputs</i>
Fire accuracy rating for FE LS8 RT products

4.5.2 Introduction

The FE Fire Products Service constitutes of a daily email service providing alerts of fire reports. The email alerts consist of QuickLook .jpeg images of the reported fires alongside KMZ archive files which contain KML files of the fire reports.

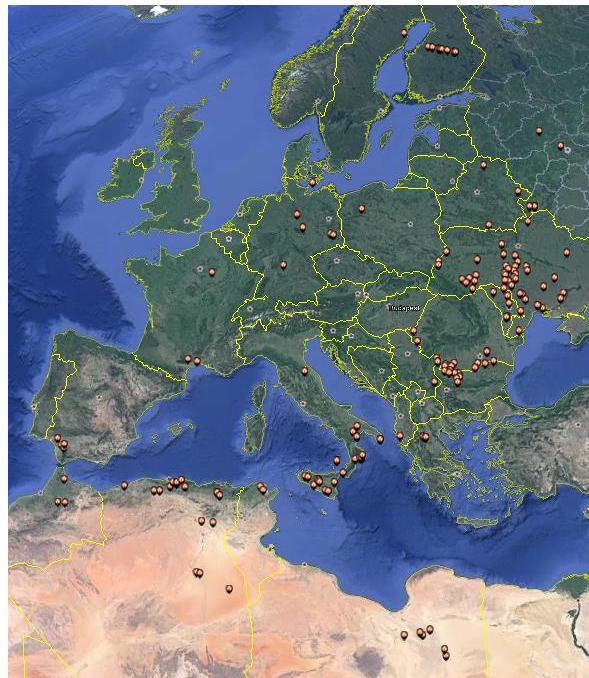


Figure 4-15: Geographical extent of all reported fires as displayed in Google Earth with individual fires denoted by markers

A three-month period of FE Fire Mosaic data ranging from 20th July 2019 to September 2019 was supplied for quality assurance and to be compared with EFFIS fire markers to assess the accuracy of the fire markers; data from earlier in July was not available as this FE instance was deployed on 20 July 2019. Additional verification was undertaken utilising visual inspections of the supplied imagery and surrounding area to determine if an accurate fire report was made and a probable cause for the reported fire. From this analysis, an overall accuracy rating for the FE product can be determined.

4.5.3 Methods and Tools

The supplied FE dataset consisted of LS8 KMZ files containing KML files, which could be displayed in Google Earth or extracted with Python and the associated .jpeg QuickLooks. (one FE Fire product contained a large number of Landsat 7 products, presenting an opportunity for further analysis).

A Python script was developed to automate the extraction of data from KMZ files, this consisted of extracting tagged fire information from KML files including date-time stamps, co-ordinates and satellite information. All outputs were processed into a csv file for ease of comparison.

As KMZ files were loaded into Google Earth for analysis, the same location and time was loaded on the EFFIS Current Situation Viewer for comparison. FE KML scenes were classified with an “accurate” fire if there was at least one active fire season marker in EFFIS within a short distance (3 pixel buffer region from the edge) of the reported fire. If there was significant time difference between the EFFIS timestamp and the KML timestamp then consideration was given to see if the fire could have persisted. If the EFFIS marker was geographically located a short distance away from the reported fire, and the fire could have progressed between the reported time frames, an accurate classification was given alongside documenting what most likely caused the fire based on location.

If no markers were present in the area surrounding a reported fire entry, then it was visually inspected. If no specific cause could be isolated through visual inspection of the KML image, surrounding area on the high resolution Google Earth basemap or EFFIS fire marker, then the LS8 SWIR-1 band was assessed for bright signals. This band was chosen as the peak wavelength of a typical fire can radiate strongly in the wavelengths covered by the LS8 SWIR-1 band and as such any fires present can be inferred from high DN values present in this band.

4.5.4 Fire Classification



Figure 4-16: Image showing an example of an agricultural fire.

Agricultural fires were the most common fire type found in the dataset, with possible causes being from cut and burn techniques or caused by accident. They are easily distinguishable in the LS8 images by dark brown/black patches (burnt areas) alongside long and thin yellow / orange streaks (fire front).

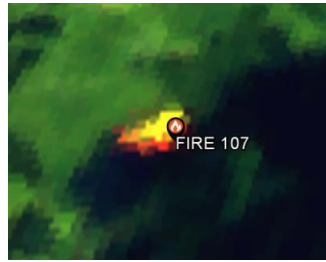


Figure 4-17: Example of a wildfire classification.

The second most common type of fire classification assigned was wildfires: varying fire shapes and some occasional fire spread with burnt areas visible. The locations for these fires greatly varied.



Figure 4-18: Image showing a reported fire over an oil refinery.

The burning of oil from refineries in desert regions and some coastal areas produced reported fire readings. The higher-resolution base map provided by Google Earth was used to identify such fires and their surroundings.

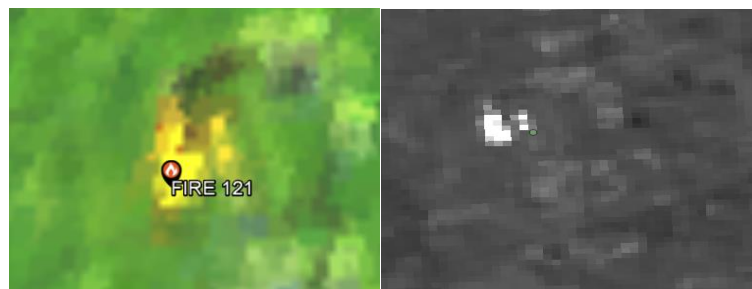


Figure 4-19: Image showing a reported fire whose likely cause is from a bright signal and associated Landsat 8 SWIR-1 band.

Bright signals were present in the dataset, easily identifiable from the distinctive shape often closely matching key features, as well as their uniform colouring. If the bright signal identified in the LS8 SWIR-1 band could not accurately verify the fire, then a false positive reading was assigned.



Figure 4-20: Image showing fire detected over urban area with unknown cause.

In very rare cases, a fire was detected over an urban area where no exact cause could be discerned from visual inspections. In these cases, the site was investigated through the LS8 SWIR-1 band.

4.5.5 Results

4.5.5.1 Summary statistics

The total number of LS8 fire scenes analysed was 152. Of those scenes, 71 (46.7%) were found to contain fires which accurately matched up with EFFIS fire markers and 81 (53.3%) scenes which did not line up to fire markers, and these are discussed below.

4.5.5.2 Fire matches

4.5.5.2.1 EFFIS matches

Table 4-7 below reports the fire classifications for the 71 products that matched with EFFIS fire markers.

Table 4-7: Fire classification for EFFIS matches

Fire Classification	Number of reported fires
Agricultural fires	42
Wildfire	19
Oil/fuel burning	9
Accident	1
Total	71

4.5.5.2.2 Non EFFIS matches

For the 81 scenes which did not match up to EFFIS markers, 74 were found to be accurate fires after visual inspection. This means that, in total, 145 (95.4%) of the provided FE dataset corresponded to accurate fires.

The largest contribution to those not present in EFFIS was found to be agricultural fires, followed by wildfires, oil burning and one fire with an accident being the most likely cause.

Of the seven scenes not corresponding to EFFIS fires nor displaying a recognisable fire from visual inspection, five were due to bright signals (from buildings and solar panels

(Figure 4-21)) and two were due to lava flows (Figure 4-22 and Figure 4-23). These are false positives.



Figure 4-21: Image showing reported fire whose shape is identical to the solar panel farm seen to the right hand side of the image.

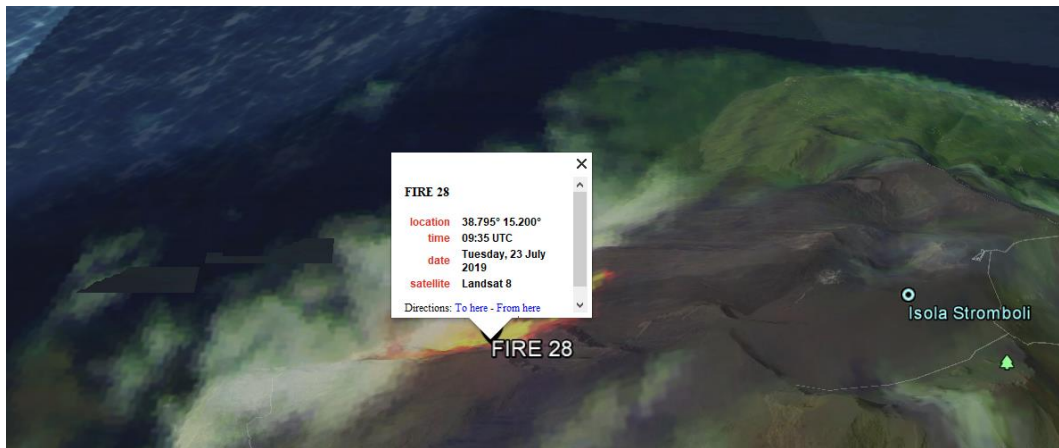


Figure 4-22: Image showing false positive detection of lava flow as a fire on 23/7/2019 at 9:35 UTC on Isola Stromboli.

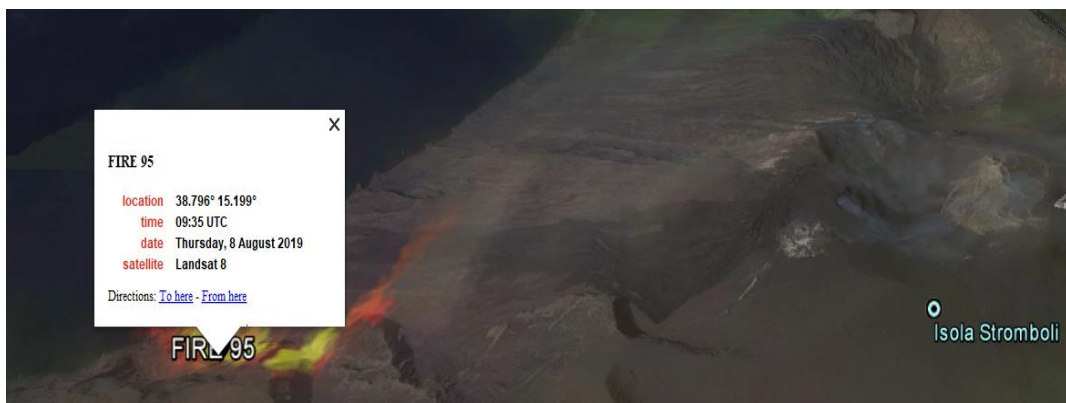


Figure 4-23: Image showing false positive detection of lava flow on 8/8/2019 at 9:35 UTC on Isola Stromboli.

The direct cause for false positives is not known, however possible causes could be due to systematic issues present in the fire detection algorithm.

Improvements in the fire detection algorithm could utilise GIS based datasets to filter out possible false positives and improve geolocation accuracy. These datasets could consist of Volcano locations derived from public datasets and if possible, distributions of solar panels. These maps could be used in comparison with reported fires as part of an automated suite, which could identify reported fires within these locations and classify them as false positive.

Additional approaches to consider in future could include investigations into utilising GFA6 datasets contained within the Copernicus Atmosphere Monitoring Service global fire assimilation system to see if this dataset can be used for additional fire verification. This approach was identified in initial investigations but not pursued due to time constraints

4.5.5.3 Geolocation Accuracy

According to [RD-1], fine geometric corrections, associated with a higher geolocation accuracy, are applied to those pixels flagged as having a fire by the FireBox algorithm only (as the geolocation information supports the required activities by the emergency services). However, this appears to have not been applied to the products procured as the mean geolocation accuracy, determined by measuring the mean displacement between the positions of these fires in the FE products and their associated position in reference Sentinel-2 products, is 604 m (ranging between 50 and 1235 m). The latter is demonstrated in Figure 4-24.





Figure 4-24: Top, FE Fire & Image product overlain on reference data; Bottom, geometric displacement of FE Fire product and reference data.



5. CONCLUSIONS

This technical note details the high-level data quality assessments (including geometric calibration, radiometric calibration and image quality) that we performed on a sample of FE LS8 OLI RT products procured from CGI.

The results of the aforementioned data quality assessments indicate an overall data quality that can be considered as generally better than expected for a real-time product (given the trade-off between quality and processing time). The results indicate data qualities that are comparable to, or better than, that reported by [RD-1] but poorer than that demonstrated by their nearest equivalent products (USGS LS8 OLI L1GS products) (e.g. geometric calibration). It is important to note that the latter results could not be reliably justified or explained in detail as FE product metadata or documentation (except for [RD-1]) does not exist or is not made available.

APPENDIX A Test Data: FE and USGS Landsat 8 OLI Products

A.1 FarEarth Landsat 8 OLI RT products

Full FE RT product dataset list available at [Error! Reference source not found.](#)

ID	Product Type	Enclosed fire report number	Product_Identifier
1	FE fire event KMZ	1, 3	20190720_090207
2	FE fire event KMZ	4	20190722_084834
3	FE fire event KMZ	5, 6, 7, 8	20190722_084933
4	FE fire event KMZ	9, 10, 11, 12, 13	20190722_085004
5	FE fire event KMZ	14, 15, 16, 17, 18, 19, 20, 21, 22, 23, 24, 25	20190722_092304
6	FE fire event KMZ	26	20190722_103002
7	FE fire event KMZ	27, 28	20190723_093521
8	FE fire event KMZ	27	20190723_093521
9	FE fire event KMZ	29, 30, 31, 32, 33, 34	20190724_083728
10	FE fire event KMZ	35	20190724_101434
11	FE fire event KMZ	36	20190724_101508
12	FE fire event KMZ	37	20190724_101557
13	FE fire event KMZ	38, 39, 40, 41, 42	20190724_101936
14	FE fire event KMZ	43	20190726_095919
15	FE fire event KMZ	44, 45, 46	20190726_100723
16	FE fire event KMZ	47	20190726_100840
17	FE fire event KMZ	48	20190727_090622
18	FE fire event KMZ	49	20190727_090822
19	FE fire event KMZ	50, 51	20190727_090935
20	FE fire event KMZ	52	20190727_091346
21	FE fire event KMZ	53	20190727_105120
22	FE fire event KMZ	54	20190728_095019
23	FE fire event KMZ	55, 56, 57, 58, 59, 60	20190729_085534
24	FE fire event KMZ	61	20190729_055611
25	FE fire event KMZ	62, 63, 64	20190729_090127
26	FE fire event KMZ	65	20190729_103450

ID	Product Type	Enclosed fire report number	Product_Identifier
27	FE fire event KMZ	66	20190729_103825
28	FE fire event KMZ	69	20190731_084408
29	FE fire event KMZ	70, 71, 72	20190731_102548
30	FE fire event KMZ	73, 74	20190802_101331
31	FE fire event KMZ	76	20190804_100101
32	FE fire event KMZ	80, 81, 82, 83, 84	20190807_084840
33	FE fire event KMZ	85, 86, 87, 88, 89, 90	20190807_084948
34	FE fire event KMZ	91, 92	20190807_085003
35	FE fire event KMZ	94	20190808_093548
36	FE fire event KMZ	95	20190808_093553
37	FE fire event KMZ	96	20190809_083744
38	FE fire event KMZ	99	20190809_101947
39	FE fire event KMZ	100	20190810_092139
40	FE fire event KMZ	101, 102, 103	20190812_090727
41	FE fire event KMZ	104	20190813_095500
42	FE fire event KMZ	105	20190822_094831
43	FE fire event KMZ	106, 107, 108	20190823_084726
44	FE fire event KMZ	110, 115	20190824_093523
45	FE fire event KMZ	111, 113	20190824_093530
46	FE fire event KMZ	112	20190824_093547
47	FE fire event KMZ	114	20190824_093607
48	FE fire event KMZ	117, 118	20190826_092017
49	FE fire event KMZ	119	20190826_092030
50	FE fire event KMZ	120, 121	20190826_092311
51	FE fire event KMZ	121	20190826_092318
52	FE fire event KMZ	123, 124, 125	20190828_090820
53	FE fire event KMZ	129	20190829_095642
54	FE fire event KMZ	130, 131	20190831_094227
55	FE fire event KMZ	132, 133	20190902_092742
56	FE fire event KMZ	133	20190902_092946

ID	Product Type	Enclosed fire report number	Product_Identifier
57	FE fire event KMZ	135	20190904_105718
58	FE fire event KMZ	136, 137, 138, 139, 140	20190904_105742
59	FE fire event KMZ	141	20190907_094836
60	FE fire event KMZ	142	20190908_084939
61	FE fire event KMZ	144	20190908_085025
62	FE fire event KMZ	145,146	20190911_110257
63	FE fire event KMZ	147, 148, 149, 150, 151, 152, 153	20190913_090828
64	FE fire event KMZ	155, 157, 158	20190915_085721
65	FE fire event KMZ	156, 159	20190915_085721
66	FE fire event KMZ	161	20190915_103626
67	FE fire event KMZ	164, 165, 166, 167, 168	20190916_094232
68	FE fire event KMZ	175	20190920_091559
69	FE fire event KMZ	179, 180	20190926_083537
70	FE fire event KMZ	181	20190926_101539
71	FE fire event KMZ	182, 183	20190927_110306
72	FE fire event KMZ	186, 187	20190928_100322
73	FE fire event KMZ	188	20190928_100859
74	FE fire event KMZ	189, 190, 191, 192, 193, 194, 196, 197	20190929_090952
75	FE fire event KMZ	195	20190929_091105
76	FE fire event KMZ	201	20190930_095319

A.2 USGS Landsat 8 OLI Products

Full USGS L1GS test dataset list

Date	USGS ID
29/01/2014	LC08_L1GS_181040_20140129_20170426_01_T1
02/03/2014	LC08_L1GS_181040_20140302_20170425_01_T1
03/04/2014	LC08_L1GS_181040_20140403_20170424_01_T1
22/06/2014	LC08_L1GS_181040_20140622_20170421_01_T1
08/07/2014	LC08_L1GS_181040_20140708_20170421_01_T1
24/07/2014	LC08_L1GS_181040_20140724_20170421_01_T1
09/08/2014	LC08_L1GS_181040_20140809_20170420_01_T1



25/08/2014	LC08_L1GS_181040_20140825_20170420_01_T1
10/09/2014	LC08_L1GS_181040_20140910_20170419_01_T1
26/09/2014	LC08_L1GS_181040_20140926_20170419_01_T1
28/10/2014	LC08_L1GS_181040_20141028_20170418_01_T1
29/11/2014	LC08_L1GS_181040_20141129_20170417_01_T1
31/12/2014	LC08_L1GS_181040_20141231_20170415_01_T1
17/02/2015	LC08_L1GS_181040_20150217_20170412_01_T1
05/03/2015	LC08_L1GS_181040_20150305_20170412_01_T1
21/03/2015	LC08_L1GS_181040_20150321_20170411_01_T1
06/04/2015	LC08_L1GS_181040_20150406_20170410_01_T1
22/04/2015	LC08_L1GS_181040_20150422_20170409_01_T1
08/05/2015	LC08_L1GS_181040_20150508_20170409_01_T1
24/05/2015	LC08_L1GS_181040_20150524_20170408_01_T1
09/06/2015	LC08_L1GS_181040_20150609_20180527_01_T1
25/06/2015	LC08_L1GS_181040_20150625_20170407_01_T1
11/07/2015	LC08_L1GS_181040_20150711_20170407_01_T1
27/07/2015	LC08_L1GS_181040_20150727_20170406_01_T1
28/08/2015	LC08_L1GS_181040_20150828_20170405_01_T1
13/09/2015	LC08_L1GS_181040_20150913_20170404_01_T1
15/10/2015	LC08_L1GS_181040_20151015_20170403_01_T1
31/10/2015	LC08_L1GS_181040_20151031_20170402_01_T1
02/12/2015	LC08_L1GS_181040_20151202_20170401_01_T1
24/04/2016	LC08_L1GS_181040_20160424_20170326_01_T1
11/06/2016	LC08_L1GS_181040_20160611_20170324_01_T1
13/07/2016	LC08_L1GS_181040_20160713_20170323_01_T1
29/07/2016	LC08_L1GS_181040_20160729_20180527_01_T1
30/08/2016	LC08_L1GS_181040_20160830_20170321_01_T1
01/10/2016	LC08_L1GS_181040_20161001_20170320_01_T1
17/10/2016	LC08_L1GS_181040_20161017_20170319_01_T1
02/11/2016	LC08_L1GS_181040_20161102_20170318_01_T1
04/12/2016	LC08_L1GS_181040_20161204_20170317_01_T1
20/12/2016	LC08_L1GS_181040_20161220_20180527_01_T1
05/01/2017	LC08_L1GS_181040_20170105_20170312_01_T1



[END OF DOCUMENT]